Journal of Engineering Science and Technology
Vol. 18, No. 2 (2023) 1237 - 1257

INFLUENCE OF PARAFUNCTIONAL LOADING CONDITIONS ON THE BIOMECHANICAL BEHAVIOUR OF DENTAL IMPLANT

MUHAMMAD IKMAN ISHAK[1,*], RUSLIZAM DAUD[1], SITI NOOR FAZLIAH MOHD NOOR[2], C. Y. KHOR[1], HUSNIYATI ROSLAN[2]

[1]Faculty of Mechanical Engineering & Technology, Universiti Malaysia Perlis (UniMAP), Kampus Alam UniMAP, Pauh Putra, 02600 Arau, Perlis, Malaysia
[2]Advanced Medical and Dental Institute, Universiti Sains Malaysia, Bertam, Jln. Tun Hamdan Sheikh Tahir, 13200 Kepala Batas, Pulau Pinang, Malaysia
*Corresponding Author: ikman@unimap.edu.my

Abstract

Dental implant success is strongly linked to technical overloading variables like implant material, implant macro geometries, and parafunctional oral behaviours. The configurations of occlusal loading on the prosthesis could affect the interaction of implant and bone particularly for patients having parafunctional oral habits. To date, the influence of various parafunctional loading conditions on the implant stability and neighbouring tissues is still unclear and debatable especially when implant loss is concerned. In this study, five different conditions of 300-N occlusal load that are vertical, oblique 15°, oblique 30°, oblique 45°, and lateral loads were evaluated through three-dimensional finite element analysis. A dataset of computed tomography images was analysed to model the bone tissues and furtherly processed in SolidWorks 2020 software. ANSYS 18.1 software was used to convert all geometries including implant parts into finite element models. The implant and bone models were assumed to be isotropic and anisotropic, respectively. The abutment screw was exerted with a pretension of 20 N. The findings exhibited that the oblique and pure lateral loads increased the stress value within the bone (~438 – 1262% higher) and implant body (~124 – 180% higher) as well as bone strains (~335 – 730% higher) compared to the pure vertical load. The total deformation of the implant body and abutment was also adversely affected by those loads with the increased angulation led to the critical condition with the relative data percentage difference of ~82 – 232%. Within the limitations of this study, it seems that the oblique and pure lateral loads have unfavourable effect on the biomechanical behaviours. An improved preoperative treatment planning by considering adequate occlusal loading configurations is desired to produce dental implant with optimal performance.

Keywords: Deformation, Dental implant, Finite element analysis, Parafunctional loading, Stress and strain.

1. Introduction

Dental implant is used to provide retention for a removable or fixed prothesis in prosthodontics. It is placed into the soft and hard oral tissues to replace missing teeth. A regular osseointegrated dental implant consists of three main individual parts namely abutment, abutment screw, and implant body. The dental implant attaches the prosthesis to the mandible or maxilla to disseminate the masticatory forces. This method is recognised as one of the appropriate treatment options for individuals seeking to repair lost or damaged teeth in terms of aesthetic, comfort, and function. Dental implant reported high success rate over years as shown in numerous clinical follow-up studies [1, 2].

Nevertheless, the incidence of post-insertion implant problems resulting in failures such as abutment and implant body loosening and even fracture is continuously being documented. The loosening and fracture of the abutment and abutment screw are more frequent compared to those of the implant body. Albeit the occurrence of implant body fracture is scarce that about 0.2 – 1.5% [3], its impact is greatly significant for both patient and dental surgeon [4]. The failure of implant usually requires maintenance and further corrective measures which also includes additional rehabilitation process.

Implant complications can be associated with two influencing factors which are biological-related events and technical overloading. The former is evidenced to give less negative implication on the implant behaviour than the latter. This could be due poor technical features of the implant parts that deteriorating the bone-implant attachment, followed by the lack of periodontal ligaments to withstand the masticatory activities. Unusual implant reaction towards loading may lead to peri-implant bone resorption and possibly subsequent failure of the prosthesis or implant components.

Furthermore, aesthetic compromise, change of soft tissue condition, and patient frustration are other complications of concern [5]. Thus, the interaction of implant and surrounding bones due to technical overloading factors should produce responses within the acceptable physiological limits. The diameter, length, material [3, 6] and wall thickness [7] of the implant body, parafunctional oral habits [8], and abutment height are the typical overloading factors recognised to affect the implant stability. This study highlights the effect of parafunctional oral habits on the load transfer within the implant system.

Occlusal force exerted on a dental implant is resolved into vertical and horizontal load components, similar to that on a natural tooth. The vertical force in the occluso-apical axis is parallel to the long axis of the implant, whilst the horizontal ones lie in the occlusal plane in the mesio-distal and bucco-lingual directions. Patients with parafunctional oral habits such as bruxism, clenching, and ice chewing experience a higher cyclic biting force [9, 10] which tends to cause implant fatigue failure [11]. Besides, the circumoral musculature and tongue perioral forces can induce frequent low-value horizontal loads on implant abutments, with the increase in the load magnitude is attained by tongue thrust or parafunctional oral habits [12].

According to American Academy of Orofacial Pain, bruxism is defined as “a movement disorder of the stomatognathic system characterized” [13]. Bruxism is described as one of the responsible factors for the failure of implant. There were about 20-35.9% of patients may generate higher-value forces to induce microfracture of the peri-implant bone tissues, resulting in bone loss and implant failure owing to bruxism

[14, 15]. Furthermore, Chitumalla et al. [16] revealed in a 5-year retrospective analysis that the survival rate of dental implants for patients with bruxism habit had declined over time, with 90, 87, 85, 75, and 72% after 1, 2, 3, 4, and 5 years, respectively. There was also contradict finding found in literature such as that in a 1 – 10-year prospective study where no relationship exists between the implant failure and bruxismv [17].

A recent finding reported insignificant difference in the survival and success rates of zirconia restoration for bruxer versus non-bruxer patients [18]. It is worth mentioning that the design of the restoration type and occlusion as well as implant numbers should remain constant in the evaluation to avoid a wide range of conclusions. The inconclusive findings observed on the influence of parafunctional loading have limited the comprehension of force transfer from the implant to the adjacent bones. Critical grasp on this aspect is a must in which the assessment can be made by varying the parafunctional loading conditions to examine the biomechanical behaviours of the implant-bone complex.

According to American Academy of Implant Dentistry, there is about 500,000 dental implants are placed in the USA in a year and the number is rising [19]. A well planned pre-operative treatment and prosthetic configuration are vital to minimise the risk of implant components failure wherein the focus should be put on the biomechanical algorithm. Different techniques are available to evaluate the biomechanical behaviours of implant and adjacent bones during the development of modern implant dentistry in conjunction with the progression of technology. Analysis of load-bearing structure has so far reached inconclusive findings, seeking for more invasive and expensive techniques to obtain more convincing solutions.

Currently, randomised and prospective trials on human are limited owing to ethical factor [19]. Instead, laboratory experimental works such as histomorphometric analysis [20], reverse torque test, photoelastic test [21], strain gauge-based assessment, and implant pull-out and push-in tests [22] are of interest in order to examine the strength and resistance of dental fixtures towards simulated physiological loadings. However, intricate anatomical shape and dimension of the structures are usually compromised that may lead to less accurate results obtained. Alternatively, basic scientific method and theoretical models are used.

Computational engineering simulation presently is a well-accepted method for analysing the mechanical behaviour of biological tissues like stress and strain levels. This method is less complicated and highly flexible compared to actual experimental works. Finite element analysis (FEA) is widely utilised simulation technique in implant dentistry that allows researchers to predict the responses which are difficult to be defined in *in vivo* and *in vitro* works [6, 23-27]. Besides, FEA provides an improved explanation for mathematical modelling problems in variety of scientific and technological fields such as thermal, structural, fluid, and fracture mechanics [28, 29]. With regard to the scope of our study, only a few recent investigations were found which discussed the influence of parafunctional loading via computational analysis. Several deficiencies have been identified and they are shown in Table 1.

Considering all the aforementioned concerns, this study was therefore aimed to analyse the biomechanical responses of a dental implant in the forms of stress, strain, and deformation under five different conditions of parafunctional occlusal loading which are vertical, oblique 15°, oblique 30°, oblique 45°, and lateral loads via three-dimensional (3-D) FEA. The oblique and lateral loads indicate the

variation of parafunctional oral habits represented by different magnitudes and directions. The null hypothesis of this study is that the value and direction of parafunctional loading do not matter to biomechanical responses. The novelty of our study was to provide clinicians with recommendations and meaningful insights of quantitative response data that could be useful in the preoperative planning of patient's occlusion prior to implant placement. It is also expected that the present study may offer an enhanced understanding on force transmission between the implant and the bone. This could subsequently address the problem of implant unpredictability that yields to failure due to overloading.

Table 1. Summary of deficiencies of the selected recent studies on parafunctional loading.

No.	Studies	Deficiencies
1	Borges Radaelli et al. [30]	The value of horizontal force component for the parafunctional load was insignificantly different with that of normal load. Also, no variation in the parafunctional load values investigated.
2	Torcato et al. [31]	Only one condition of the parafunctional load was studied. Besides, the value of vertical force component (1000 N) was quite high for the implanted patient case.

2. Materials and Methods

2.1. Three-dimensional mandibular bone model development

A 3-D model of mandibular bone was constructed based on a series of computed tomography (CT) image datasets of a craniofacial using an image-processing software, Mimics 20.0 (Materialise, Leuven, Belgium). In this study, only one CT image dataset of real craniofacial was considered. There were two different layers of bone developed which are cortical and cancellous. These two bone structures were distinguished using threshold tool indicated by different bone density scale value. The region of interest was selected to be the left part of the mandible model, which included the second molar, first molar, and second premolar. The existence of the mandibular canal at the superior portion was disregarded in the analysis. To verify the accuracy of the bone model created, a comparison was made with the virtual mandibular bone model from a 3-D human anatomy software, Complete Anatomy from 3D4Medical, Elsevier. A few modifications have been imposed on the bone model such as flattening the mesial, distal, superior, and inferior parts due to limited computing resource to process the complex geometrical shape. Besides, the simplification was done to prevent the development of poor or highly distorted elements in the numerical analysis stage later. As a result, the finalised bone model has a width of 8 – 10 mm, length of 30 mm, height of 20 mm, and thickness of 2 mm (cortical layer). These dimensions are in agreement with those shown in some previous published computational studies that simulating the same bone region of interest [32, 33].

The cancellous bone is a porous structure; however, it has been designed as a solid continuum body and assigned with spongy material properties in this study. The cortical bone is denser, and it surrounds the cancellous bone. The first molar tooth was extracted to imitate implant body insertion in bone at that location. The other two teeth – the second molar and second premolar – were also removed and

the affected regions were closed and left unattended. The prosthesis or crown model was designed from the geometry of the coronal part of the first molar by using Boolean operation. Since the prosthesis model constitutes a framework layer, therefore, its configuration was represented by reducing the prosthesis dimensions about 30%.

2.2. Three-dimensional implant model development

A computer-aided design (CAD) software, SolidWorks 2020 (SolidWorks Corp., Concord, Massachusetts, USA) was employed to create the 3-D model of the abutment, abutment screw, and implant body. All dimensions used were compliant with those of dual-fit implant (DFI) (Alpha-Bio Tec, Petach Tikva). The length of the implant body is 11.5 mm, and the diameter is 3.75 mm. As for the implant-abutment connection, the internal hexagonal type was adopted. Whilst the implant thread shape had been modelled as V-shaped type. The abutment fixedly holds the prosthesis in place, and it is attached to the implant body via an abutment screw. The abutment is 3.5-mm high, while the abutment screw is 8- and 2.2-mm long and wide, respectively. Relevant SolidWorks in-built geometry tools such as sweep, extrude, revolve, and loft were utilised to develop all implant part models. To substantiate the accuracy of model construction, a verification was made by comparing all the 3-D model designs with the real dimensions and tolerances provided in the catalogue of implant manufacturer. Figure 1(a) shows the exploded configuration of the implant component models.

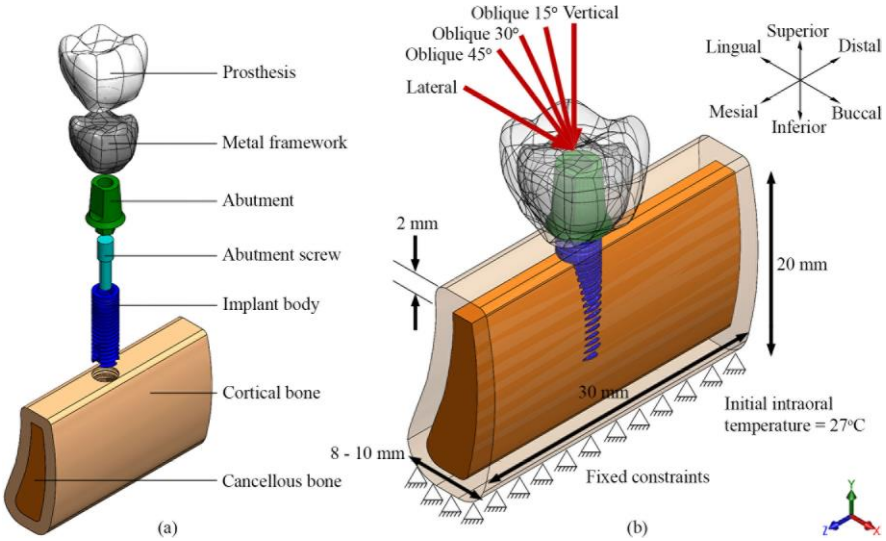

Fig. 1. (a) Exploded view of implant-bone assembly. (b) The bottom surface of the cortical bone is fixed in all directions and different parafunctional loading conditions subjected to the top surface of the prosthesis.

2.3. Virtual surgery simulation

Prior to the insertion of the implant body into the bone, the implant part and bone models must be converted into solid geometries. This process was executed in SolidWorks software. The implant body was inserted into the bone model based on

the bone-level approach, by which the flat surface of implant platform was positioned and set parallel to the top surface of the cortical bone. The rationale behind this is to warrant a satisfactory outcome of prosthesis orientation. The bone bed with a width of 3.75 mm was then prepared by using "combine" feature through "subtract" tool.

2.4. Contact modelling

To designate a full osseointegration of the implant body to the surrounding bones, the entire interfaces of the implant-to-bone were simulated to be perfectly bonded. This method was also normally observed in many earlier *in-vitro* works [34-36]. It indicates the direct contact approach to inhibit any relative displacements at the interface. The similar contact method was considered for the attachment between the cancellous and the cortical bones. On the contrary, all the contact surfaces presented among the prosthetic and implant components were assumed to be frictional by adopting the friction coefficient, μ of 0.3 [37]. Augmented Lagrange method was the contact algorithm applied at the related surfaces which automatically managed by the program. In addition, the contact detection was described by Gaussian integration point.

2.5. Material properties assignment

The bone models were assumed to be anisotropic, while the implant part models were assigned with isotropic properties. The strength of the bone is mainly associated with the orientation of collagen fibres in its structure. The modulus of elasticity of the mandibular cortical layer is the lowest along the corono-apical or bucco-lingual direction (90º, transverse) and the highest along the mesio-distal direction (0º, longitudinal). To date, many computational studies have considered the anisotropic biological tissue properties to obtain more reliable findingsv [38-40]. The material characteristics of all finite element models utilised in the analysis are shown in Table 2.

Table 2. Material properties of each finite element model.

Material	Model	Elastic Modulus, E (GPa)	Poisson's Ratio, v	Shear Modulus, G (GPa)	References
Ti-6Al-4V	Abutment, abutment screw & implant body	113.8	0.342	-	Yalçın et al. [32]
Feldspathic porcelain	Prosthesis	82.8	0.35	-	Tekin et al. [41]
CoCr alloy	Framework	218	0.33	-	Elias et al. [42]
Cortical bone	-	E_x = 17.9 E_y = 12.5 E_z = 26.6	v_{yz} = 0.31 v_{xy} = 0.26 v_{xz} = 0.28	G_{yz} = 5.3 G_{xy} = 4.5 G_{xz} = 7.1	Robau-Porrua et al. [39]
Cancellous bone	-	E_x = 1.148 E_y = 0.021 E_z = 1.148	v_{yz} = 0.055 v_{xy} = 0.003 v_{xz} = 0.322	G_{yz} = 0.068 G_{xy} = 0.068 G_{xz} = 7.100	Robau-Porrua et al. [39]

2.6. Loading and boundary conditions

Two main loading configurations were included in the present study which are screw pretension and occlusal load. The screw pretension was represented by a force of 20 N [32] which subjected to the outer surfaces of the abutment screw. For the occlusal load, five different loading sets – vertical (0°) [32], oblique 15° [43], oblique 30° [33], oblique 45° [44], and lateral (90°) [45] loads – with a resultant force value of 300 N [32] were investigated, in which each loading case is differed in terms of force component magnitudes and direction. The oblique and lateral loads represent the variation of parafunctional loadings while the vertical load indicates a controlled loading case. All the loads were exerted on the top surface of the prosthesis. The angle of oblique loads was set away from the vertical implant axis (*y* axis). To clearly manifest the magnitude of each load, the resultant load (300 N) was resolved into vertical (*y* axis) and horizontal components (*x* and *z* axes) especially the oblique ones as exhibited in Table 3. It was shown that the increase in the loading angle has increased the horizontal force component accordingly and the reverse was seen for the vertical force component. This simulated the clinical situation where patient with severe parafunctional oral habits tends to increase the level of horizontal force. The initial temperature of environment or intraoral condition was set to 27°C. For the boundary conditions, a fixed constraint was determined at the bottom surface of the bone model in all directions (*x*, *y*, and *z* axes) to limit the displacement for the attached part [32]. The boundary conditions and occlusal loading configurations are depicted in Fig. 1(b).

Table 3. Force components of five different occlusal loading configurations excluding the screw pretension which was set similar in all cases.

Loading	Vertical Component	Horizontal Component
Vertical	F_y = 300 N	F_x = 0 N; F_z = 0 N
Oblique 15°	F_y = 289.78 N	F_x = 54.9 N; F_z = 54.9 N
Oblique 30°	F_y = 259.8 N	F_x = 106.06 N; F_z = 106.06 N
Oblique 45°	F_y = 212.14 N	F_x = 150 N; F_z = 150 N
Lateral	F_y = 0 N	F_x = 212.13 N; F_z = 212.13 N

2.7. Finite element model verification

Mesh convergence test was conducted to ensure the solutions of FEA are free from all purely numerical factors. Before undergoing the mesh convergence test, the FEA models were converted into solid tetrahedral elements in ANSYS 18.1 software (ANSYS Inc., Houston, TX, USA). Each tetrahedral element comprises four nodes with three degrees of freedom. A total of six different mesh density sets was prepared – Tet-A: 190,000 elements; Tet-B: 260,000 elements; Tet-C: 410,000 elements; Tet-D: 750,000 elements; Tet-E: 1,083,000 elements; and Tet-F: 1,690,000 elements. The process was executed by using automatic solid meshing function in ANSYS software. Each model set was assigned with isotropic, homogenous, and linearly elastic material properties (cortical bone: E = 13.7 GPa, ν = 0.3; cancellous bone: E = 1.37 GPa, ν = 0.3; Ti-6Al-4V (implant parts): E = 113.8 GPa, ν = 0.342; feldspathic porcelain (prosthesis): E = 82.8 GPa, ν = 0.35; and CoCr alloy (framework): E = 218 GPa, ν = 0.33). All the contact surfaces were assumed to be bonded. A 300-N vertical load was applied on the top surface of the prosthesis and a 20-N screw pretension was exerted on the abutment screw. The bottom surface of the cortical bone model was fully constrained. All trials in the convergence test were assessed in terms of the maximum principal stress data recorded within the bone. The results

demonstrated that there was an insignificant change of the stress magnitudes generated between the finest and other coarser models. The model seemed to converge after one refinement with the maximum change of 2.7% at the total number of nodes and elements of about 400,000 and 260,000, respectively. Figure 2 exhibits a plot of the maximum principal stress and mesh configuration created in the model before (Tet-A) and after one refinement (Tet-B).

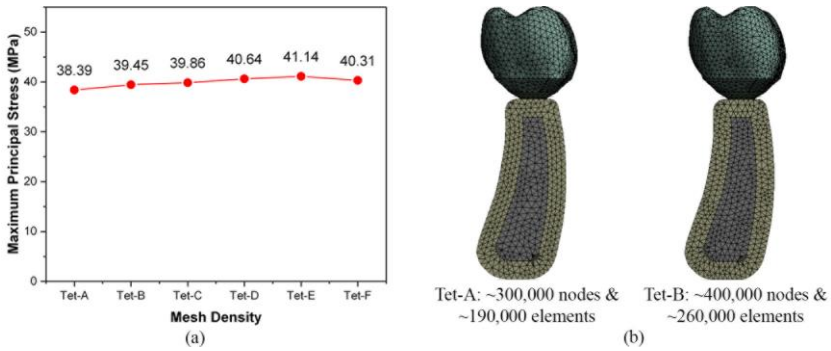

Fig. 2. (a) Plot of maximum principal stress vs. mesh density. (b) Mesh distribution between Tet-A (before) and Tet-B (after one refinement).

The selected mesh condition of the finite element model was then compared with earlier works that analysing similar restoration type and implantation site for verification purpose. A replication was made on the input settings used in those studies excluding the geometrical shape of models. The difference in terms of total number of elements was insignificant because we only considered the studies that used the same region of interest. The comparison was made in terms of equivalent von Mises stress value generated in the bone. It was evidenced that the highest stress magnitude recorded between our model and past investigations was comparable as shown in Table 4.

Table 4. Comparison of maximum equivalent von Mises stress results in the bone between the proposed model and literature.

Studies	Proposed Model Results	Literature Results
Yalçın et al. [32]	29.93 MPa	20.93 MPa
Schwitalla et al. [33]	19.13 MPa	17.00 MPa

2.8. General formulations

In the present study, a non-linear FEA was performed to solve the problem. The non-linearity aspect was covered in the contact modelling where frictional contact interfaces were assigned among the prosthetic components via friction coefficient value. This has resulted in the change of structure stiffness upon the application of loadings. A finite element method solves simultaneous algebraic equations using matrix methods that indicating a reference state of structure on equilibrium path. This study solves the nodal displacement vector $\{u\}$ using the overall equilibrium equation shown in Eq. (1) [46].

$$[K(u)]\{u\} = \{F(u)\} \quad (1)$$

The notation K is total stiffness matrix and F is total applied load vector. Both stiffness and applied load are a function of displacement. Newton-Rapson method was used to solve the non-linear problem by computing displacement increments in each iteration based on tangent stiffness. For an example, the displacement increments at iteration 1 Δu_1 can be described as in Eq. (2) [46]:

$$\{\Delta u_1\}[k_{t1}] = \{F_a\} - \{F_1\} \tag{2}$$

where Δu_1 is displacement increment at iteration 1 and $k_{t1} = k_0 - k_{n1}$ is updated tangent stiffness at iteration 1. Then, the displacement vector for the next iteration (i.e., iteration 2 u_2) is given by Eq. (3) [46].

$$\{u_2\} = \{u_1\} + \{\Delta u_1\} \tag{3}$$

For any iteration j, the displacement increment and corresponding displacement vector can be expressed as in Eq. (4) and Eq. (5), respectively [46].

$$\{\Delta u_j\}[k_{tj}] = \{F_a\} - \{F_j\} \tag{4}$$

$$\{u_{j+1}\} = \{u_j\} + \{\Delta u_1\} \tag{5}$$

The deformation of the structure was determined based on the nodes by which any point displacement vector is interpreted in three components as shown in Eq. (6) [47].

$$\{u\} = [u \quad v \quad w]^T \tag{6}$$

The stress and strain vectors at a point in this 3-D elastic problem are expressed as in Eq. (7) and Eq. (8), respectively [47].

$$\{\sigma\} = [\sigma_x \quad \sigma_y \quad \sigma_z \quad \tau_{yz} \quad \tau_{xz} \quad \tau_{xy}]^T \tag{7}$$

$$\{\varepsilon\} = [\varepsilon_x \quad \varepsilon_y \quad \varepsilon_z \quad \gamma_{yz} \quad \gamma_{xz} \quad \gamma_{xy}]^T \tag{8}$$

The stress-strain relation is given by Eq. (9) [47]:

$$\{\sigma\} = [D]\{\varepsilon\} \tag{9}$$

where $[D]$ is stress-strain matrix.

The risk of bone failure was predicted based on normal stress behaviours through maximum-normal-stress failure theory for a non-ductile material [42]. If the principal stresses for a general stress state are arranged in the ordered form $\sigma_1 \geq \sigma_2 \geq \sigma_3$ [48], failure is predicted to occur whenever,

$$\sigma_1 \geq S_{ut} \qquad \text{or} \qquad \sigma_3 \leq -S_{uc} \tag{10}$$

where S_{ut} and S_{uc} are the ultimate tensile and compressive strengths, respectively, given as positive quantities.

The von Mises stress, on the other hand, was used to predict the occurrence of yielding when the distortion strain energy per unit volume reaches or exceeds the distortion strain energy per unit volume for yield. This criterion was applied for the justification of implant body response in this study. For the general state of stress, yield is predicted to occur as exhibited in Eq. (11) [48]. The notation S_y indicates the yield strength of the material.

$$\left[\frac{(\sigma_1-\sigma_2)^2+(\sigma_2-\sigma_3)^2+(\sigma_3-\sigma_1)^2}{2}\right]^{1/2} \geq S_y \tag{11}$$

3. Results

The maximum principal stress (bones), equivalent von Mises stress (implant body), maximum principal strain (bones), and total deformation (abutment-implant body complex) were extracted in the post-processing analyses in order to scrutinise the issue investigated. The maximum principal stress was applied to structurally predict the response of the bones due to the difference in the effect of mechanical stresses for a friable (non-ductile) material [42]. The equivalent von Mises stress, on the other hand, quantitatively estimates the stress of a point as a non-uniaxial stress rate, which suitable to display the results of the computations of ductile material. This criterion has also extensively been accepted and applied in many previous computational studies [32, 34, 42]. Besides, the findings were also presented in spectrum colouring scale with red representing high stress, strain, or total deformation magnitude, while blue representing low magnitude. The major findings of the investigation are summarised in Table 5 for each loading case.

Table 5. Values of the stresses, strain, and total deformation in all loading sets.

Loading	Maximum Principal Stress (MPa)	Equivalent von Mises Stress (MPa)	Maximum Principal Strain	Total Deformation (µm)
Vertical	47.88	612.89	3,351.1 µ	113.09
Oblique 15°	652.26	1415.48	27,815 µ	40.84
Oblique 30°	646.38	1393.81	27,695 µ	109.57
Oblique 45°	642.50	1375.33	27,630 µ	205.69
Lateral	257.77	1715.40	14,572 µ	375.58

3.1. Maximum principal stress results

Bone stress was significantly increased with the presence of horizontal load components in the occlusal loading with the percentage difference ranging from ~438 to 1262% higher relative to pure vertical load. It appears that oblique 15° load recorded the highest stress value (652.26 MPa) as compared to vertical (47.88 MPa), oblique 30° (646.38 MPa), oblique 45° (642.5 MPa), and lateral loads (257.77 MPa). The maximum bone stress magnitude produced by oblique 15° load was observed to be approximately 13.6-, 1.0-, 1.0-, and 2.5-times higher than that by vertical, oblique 30°, oblique 45°, and lateral loads, respectively. The most affected region in the bone was the cervical part, especially under the application of oblique 45° and lateral loads as exhibited in Fig. 3. Besides, the oblique loads also attributed the middle area of the bone-implant interface with excessive bone stress level.

3.2. Equivalent von Mises stress results

The results of equivalent von Mises stress in the implant body were consistent with the bone stress results. It was shown that the implant stress also increased when the horizontal load component existed, supported by the relative percentage difference from ~124 to 180%. The pure lateral load yielded the greatest implant stress (1715.4 MPa) relative to others (vertical: 612.89 MPa; oblique 15°: 1415.48 MPa; oblique 30°: 1393.81 MPa; oblique 45°: 1375.33 MPa). The

distribution of stress over the implant body corresponded well with the stress contour plot of the bone. It was revealed that the high stresses were accumulated at the implant coronal part as well as at the middle region towards the apical portion (Fig. 4). As the value of horizontal load component was increased, the critical stress regions seemed to become larger on the buccal side of the implant body. More satisfactory stress dispersions were found on the mesial and lingual sides irrespective of loading cases. Although high stress intensity areas generated by oblique 15° load was less significant and limited than those by other load conditions, its magnitude was about 1.6%, 2.9%, and 131% greater than oblique 30°, oblique 45°, and vertical loads, respectively.

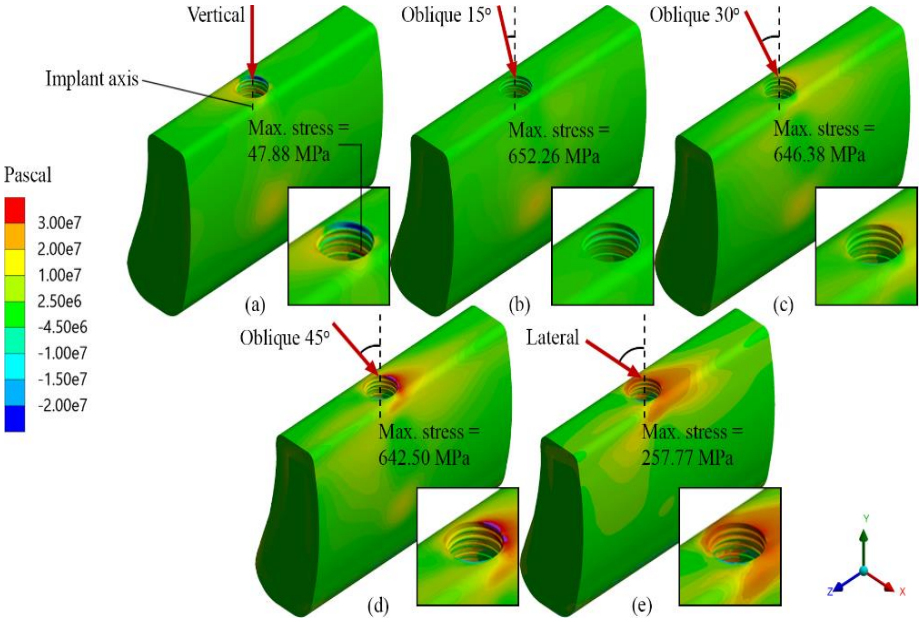

Fig. 3. Distribution of maximum principal stress in the bones for different loading configurations, (a) vertical, (b) oblique 15°, (c) oblique 30°, (d) oblique 45°, and (e) lateral loads.

3.3. Maximum principal strain results

In terms of strain measurement, the findings revealed that there was an increase in the bone strain value under the application of oblique and lateral loads. The highest bone strain magnitude was generated by oblique 15° load (27,815 μ) with less difference observed among other loads with horizontal force component (oblique 30°: 27,695 μ; oblique 45°: 27,630 μ) except pure lateral load (14,572 μ). The pure vertical load merely produced the bone strain with the maximum value of 3,351.1 μ. The percentage difference of peak bone strain between the oblique and vertical loads was from ~335 – 730%. In general, the magnitude of strain in the cortical bone was slightly higher than that in the cancellous bone regardless of loading conditions. High strain concentration was noticed at the cervical and apical regions of the bone for all cases as depicted in Fig. 5. The strains appeared to be more largely disseminated for the cases with increased horizontal load component values.

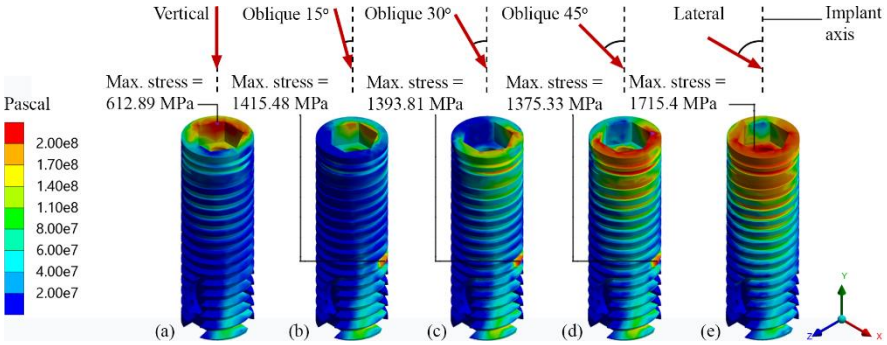

Fig. 4. Distribution of equivalent von Mises stress in the implant body for different loading configurations, (a) vertical, (b) oblique 15°, (c) oblique 30°, (d) oblique 45°, and € lateral loads.

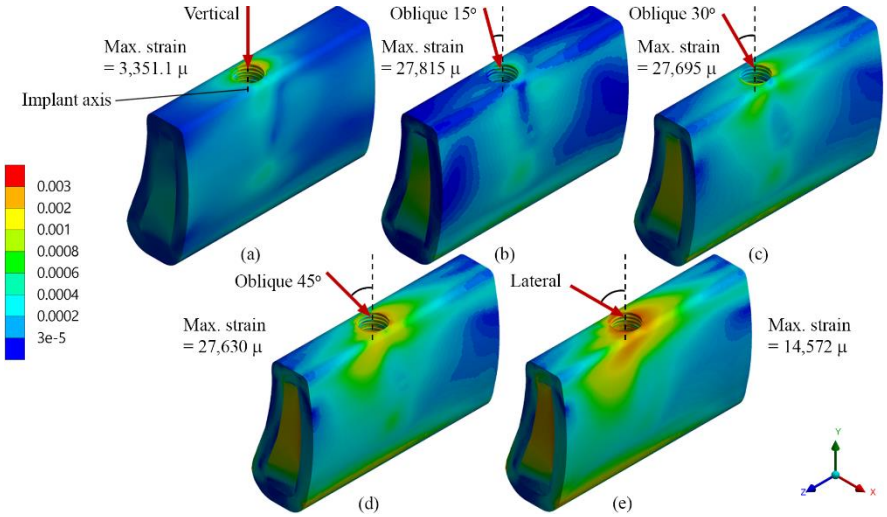

Fig. 5. Distribution of maximum principal strain in the bones for different loading configurations, (a) vertical, (b) oblique 15°, (c) oblique 30°, (d) oblique 45°, and (e) lateral loads.

3.4. Total deformation results

Our findings showed that the increase in the value of horizontal load component (from vertical to lateral load) have proportionally increased the total deformation of implant body (vertical: 16.20 μm; oblique 15°: 25.22 μm; oblique 30°: 49.58 μm; oblique 45°: 72.84 μm; lateral: 105.38 μm) as illustrated in Fig. 6. Meanwhile, the total deformation of abutment under the vertical, oblique 15°, oblique 30°, oblique 45°, and lateral loads was 113.09 μm, 40.84 μm, 109.57 μm, 205.69 μm, and 375.58 μm, respectively. It was shown that the displacement of the abutment was slightly lower under oblique 15° and oblique 30° loads than the pure vertical load. Whilst the oblique 45° and lateral loads had produced the total deformation about 82 and 232% higher than the pure vertical load, respectively. In comparison, the implant body displaced less than the abutment for all loading conditions with the percentage difference ranging from about 47% (oblique 15°) up to 150%

(vertical). Irrespective of loading configurations, the top part of the abutment on the distal side was prone to deformation. For the implant body, the critically deformed region occurred at the edge of the implant platform. A larger deformation concentration region developed towards the apical part as the load inclination increased, signifying a high tendency of implant body to dislocate starting from the coronal part.

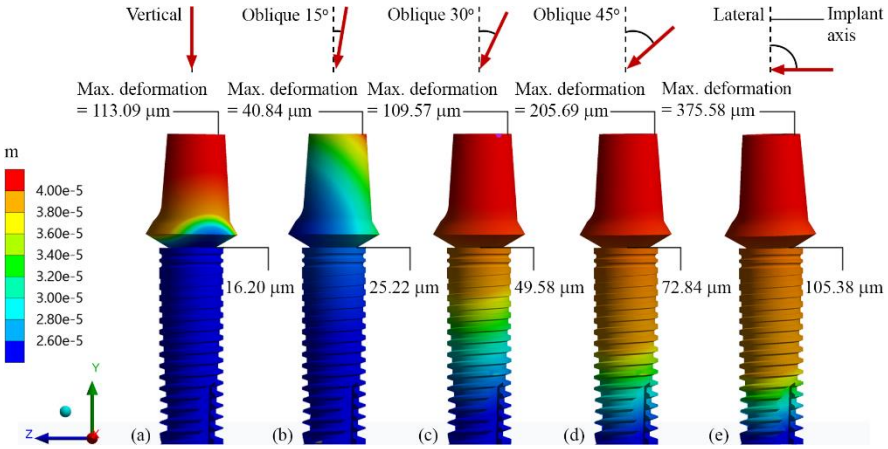

Fig. 6. Distribution of total deformation of the abutment-implant assembly for different loading configurations, (a) vertical, (b) oblique 15°, (c) oblique 30°, (d) oblique 45°, and (e) lateral loads.

4. Discussion

This study evaluated the effect of different configurations of parafunctional occlusal loading which represented by variety magnitudes of the vertical and horizontal force components on a dental fixture via 3-D FEA. The core objective was to examine whether varying loading condition may influence the limits of bone adaptation resulting in the alteration of osseointegration. The clinical perseverance of a dental fixture is considerably determined by good primary stability and lasting osseointegration which securing the implant placement in bone. Implant geometry, implantation method, implant material, and occlusal loading are among factors that can affect the performance of dental implant. In general, excessive occlusal loading by patients with bruxism could induce fatigue failure of the implant [11, 49]. Considering this, different occlusal loading configurations with variation in value and direction were analysed. The influence of vertical, oblique, and lateral loads on the force transfer from the implant to the bone is vital particularly when the stress shielding phenomenon is concerned. Bone adaptation towards loading could clearly be manifested by the understanding of the mechanics of stress transfer at the bone-implant interface.

To the extent that stress in the bones was concerned, a higher stress level was generally produced by the inclined or oblique loads (resultant occlusal load with horizontal force component) compared to the pure vertical load. This is congruent with the implant stress wherein the magnitude of stress was significantly increased. Dental implants are subjected to numerous cyclic loadings that caused by physiologic masticatory cycles and parafunctions [13]. Occlusal load tends to change its magnitude, frequency, and duration which primarily associated with

parafunctional oral habits. Patients who engage in parafunctional oral behaviours such as clenching, bruxism, and ice chewing have a higher cyclic biting force that can attribute the implant to fatigue failure [9, 10]. Loads with horizontal force component resulted in a greater stress within the bone than the pure vertical load, with oblique 15° load demonstrated the highest bone stress. This agrees well with the FE analysis findings by Kim et al. [50]. They stated that the loading of 100 N (15°) produced higher implant stress (677.28 and 687.80 MPa) as compared to the axial load (257.16 and 304.65 MPa) for different implant designs investigated. Meanwhile, for the implant body, pure lateral load led to the most superior bone stress. The findings were consistent with a work by Marcián et al. [51] which reported that the presence of lateral forces resulted in an unfavourable impact on the implant and surrounding bones. Another study drew similar conclusion where the oblique 150 N-load (45°) resulted in a higher trabecular (15 MPa) and cortical bone (150 MPa) stresses relative to the vertical load (trabecular: 6 MPa; cortical: 73 MPa) [52]. Overall, the maximum bone stress recorded in the analysis for all loading conditions was greater than the reported strength of cortical bone, 170 MPa, except the one under the vertical load. This could predict potential failure of the bone. Peri-implant or marginal bone loss is one of the primary manifestations in current implant dentistry concerning osseoinsufficiency [53]. This phenomenon can occur early or late during the service of dental implant. Critical marginal bone loss may cause hard and soft tissues deformation, aesthetic compromise, patient dissatisfaction, and implant extraction [5]. It was generally reported that the height of marginal bone decreased about 1.0 mm in the first year of implant insertion. In the subsequent years, the bone level was reduced about 0.2 mm [5]. The resorption of supporting bone around an implant could lead to the eventual implant removal. Among the complications associated with the bone loss are implant body loosening and fracture which may put the patients, for the worst case, in psychological trauma and financial loss. As such, peri-implant bone loss should be kept at minimum such as by attaining adequate mechanical stress transfer from the implant to the bone.

For the implant body, the maximum von Mises stress value generated was slightly higher than the yield strength of the implant material (Ti6Al4V), 900 MPa, expecting the degradation of implant perseverance. In terms of stress distribution pattern within the implant body, our findings exhibited that the middle region especially at the sharp edge of the apical groove also sustained high stress concentration, not only the cervical or neck region as commonly reported in previous studies. Therefore, a high concern should not only be given to the cervical region for improved stress adaptation, but also to the middle-to-apical regions. Of all loading conditions, occlusal load at the angulation of 15° appears to be greatly affecting the bone, while the pure lateral occlusal load put the implant body in a high risk of failure.

Strain intensity in the bones is another crucial element for the justification of bone response towards loading apart from the mechanical stresses. Our findings exhibited that the magnitude of bone strain was increased as the horizontal load component is present. Among oblique loads, the bone strain was the highest under the application of loading at 15°. This seems to be parallel with a previous study by Marcián et al. [51] where the buccolingual (lateral) forces critically strained the adjacent bones as compared to the axial load. However, the reported strain magnitudes were lower than those of this study due to different force value (150 N) and geometrical model used. Similar conclusion was found in a later study where the vertical load demonstrated less tendency of bone loss as compared to the

oblique load [54]. To relate the recorded strains with bone responses, Frost's mechanostat theory is adopted [35, 55]. It was revealed that only strain value generated in the cortical bone by the vertical load lies in the range of 2,500 μ – 4,000 μ which predicting physiologic overload based on Frost's mechanostat theory. As other bone strains were greater than 4,000 μ, they are expected to experience pathologic overload. The findings do not correspond well with common clinical observations. Based on the findings, other strain threshold classes may suitably be considered for the justification of the alveolar bone strains.

The ability of a dental fixture to be free of clinical movement is expressed as its stability. The implant stability is also known as the ability of a fixture to sustain the lateral and axial loads, as well as rotational load. In this study, it is noteworthy that the total deformation of the implant body was increased with the increase in the loading inclination. As far as the movement of the implant body is concerned, all the recorded values were not exceeding the tolerable range of implant motion which is from 50 to 150 μm [56]. If the implant motion is far-off this range, it could impair the bone-implant connection because of the development of fibrous tissues. As for the abutment, similar observations were recorded where the inclined loads caused superior dislocation. Higher displacement magnitudes generated in the abutment than those in the implant body regardless of loading conditions could be due to the adjacent location of the loading point with the abutment that increases the bending deformation. Good structural integrity of the abutment or its screw is important and must be retained because the failure of this structure may trigger other following destructions. Based on a study by Beschnidt et al. [57], it was reported that the loosening of abutment screw has contributed to the movement of prosthesis. The problem was then successfully fixed by retightening the screw. For the critical loosening, implant body fracture could occur [58]. High deformation is also expected from the inclined loads due to the increase in the horizontal load values that leading to a more significant motion.

Despite the robust findings of this study, a few criteria can further be improved such as considering different dimensions of the implant body, applying different types of implant material, and reversing implant removal from the bony socket. The present study had several limitations: (1) the gingiva soft tissue and mandibular canal were ignored; (2) the occlusal loading was only applied at one specific location; (3) the morphological features of the bone model were simplified; and (4) only the first molar of the mandible was analysed, in which the results are solely attributable to this type of restoration. The present finding could not be extrapolated straightforwardly to real clinical conditions, but it may disclose the difference in the biomechanical behaviours using computational modelling. *In vitro* and/or *in vivo* clinical studies are necessary to be performed to motivate and validate the results of analysis based on regulatory standards. This study served to reject the null hypothesis we made earlier. We managed to demonstrate that the value and direction of the parafunctional loading have an important influence on biomechanical responses.

5. Conclusions

The results of non-linear computational analysis support the following conclusions.

- The oblique and pure lateral loads showed an increased stress value within the bone and implant body for about 438 – 1262% and 124 – 180%, respectively, compared to the pure vertical load.

- Moreover, the oblique and pure lateral loads promoted approximately 335 – 730% higher bone strain magnitude than the pure vertical load.
- The total deformation of the implant body and abutment was also adversely affected by the oblique and lateral loads with the increased angulation or value led to the most critical implant condition. This is supported by the relative data percentage difference recorded which was about 82 – 232% increase.
- An improved preoperative treatment planning in terms of patient's occlusion condition is anticipated to produce dental implant with optimal performance that could subsequently minimise the risk of implant failure.

Acknowledgements

The authors would like to acknowledge the support from the Fundamental Research Grant Scheme (FRGS) under a grant number of FRGS/1/2020/TK0/UNIMAP/03/2 from the Ministry of Higher Education Malaysia. The authors reported no conflicts of interest related to this study.

Nomenclatures

D	Stress-strain matrix
E	Elastic modulus, GPa
F	Applied load, N
G	Shear modulus, GPa
j	Iteration number
K	Stiffness
k_0	Initial tangent stiffness
k_t	Updated tangent stiffness
S_{uc}	Ultimate compressive strength, MPa
S_{ut}	Ultimate tensile strength, MPa
S_y	Yield strength, MPa
u	Displacement, displacement in x axis, m
v	Displacement in y axis, m
w	Displacement in z axis, m

Greek Symbols

Δu	Displacement increment
ε	Normal strain
μ	Friction coefficient
ν	Poisson's ratio
σ	Normal stress, MPa

Abbreviations

3-D	Three-Dimensional
CAD	Computer-Aided Design
CT	Computed-Tomography
DFI	Dual-Fit implant
FEA	Finite Element Analysis
3-D	Three-Dimensional

References

1. Pal, T. (2015). Fundamentals and history of implant dentistry. *Journal of International Clinical Dental Research Organization*, 7(3), 6-12.
2. Agustin-Panadero, R.; Leon-Martinez, R.; Labaig-Rueda, C.; Faus-Lopez, J.; and Sola-Ruiz, M.F. (2019). Influence of implant-prosthetic connection on peri-implant bone loss: A prospective clinical trial with 2-year follow-up. *The International Journal of Oral & Maxillofacial Implants*, 34(4), 963-968.
3. Chrcanovic, B.R.; Kisch, J.; Albrektsson, T.; and Wennerberg, A. (2018). Factors influencing the fracture of dental implants. *Clinical Implant Dentistry and Related Research*, 20(1), 58-67.
4. Stoichkov, B.; and Kirov, D. (2018). Analysis of the causes of dental implant fracture: A retrospective clinical study. *Quintessence International*, 49(4), 279-286.
5. Naveau, A.; Shinmyouzu, K.; Moore, C.; Avivi-Arber, L.; Jokerst, J.; and Koka, S. (2019). Etiology and measurement of peri-implant crestal bone loss (CBL). *Journal of Clinical Medicine*, 8(2), 1-20.
6. Ouldyerou, A.; Merdji, A.; Aminallah, L.; Roy, S.; Mehboob, H.; and Özcan, M. (2022). Biomechanical performance of Ti-PEEK dental implants in bone: An in-silico analysis. *Journal of the Mechanical Behavior of Biomedical Materials*, 134, 105422.
7. Gupta, S.; Gupta, H.; and Tandan, A. (2015). Technical complications of implant-causes and management: A comprehensive review. *National Journal of Maxillofacial Surgery*, 6(1), 3-8.
8. Kunjappu, J.J.; Mathew, V.B.; Abdul Kader, M.M.; Kuruniyan, M.S.; Ali, A.B.M.; and Shamsuddin, S.V. (2019). Fracture of dental implants: An overview. *International Journal of Preventive and Clinical Dental Research*, 6(1), 21-23.
9. Bayata, F.; and Yildiz, C. (2020). The effects of design parameters on mechanical failure of Ti-6Al-4V implants using finite element analysis. *Engineering Failure Analysis*, 110, 104445.
10. Soo, S.Y.; Silikas, N.; and Satterthwaite, J. (2019). Measurement of fracture strength of zirconia dental implant abutments with internal and external connections using acoustic emission. *Materials*, 12(12), 2009.
11. Shemtov-Yona, K.; and Rittel, D. (2015). On the mechanical integrity of retrieved dental implants. *Journal of the Mechanical Behavior of Biomedical Materials*, 49, 290-299.
12. Bidez, M.W.; and Misch, C.E. (2015). *Dental implant prosthetics*. Mosby.
13. Prados-Privado, M.; Prados-Frutos, J.C.; Manchón, Á.; Rojo, R.; Felice, P.; and Bea, J.A. (2015). Dental implants fatigue as a possible failure of implantologic treatment: The importance of randomness in fatigue behaviour. *BioMed Research International*, 2015, 825402.
14. Chrcanovic, B.R.; Kisch, J.; Albrektsson, T.; and Wennerberg, A. (2016). Bruxism and dental implant failures: a multilevel mixed effects parametric survival analysis approach. *Journal of Oral Rehabilitation*, 43(11), 813-823.
15. Chrcanovic, B.R.; Kisch, J.; Albrektsson, T.; and Wennerberg, A. (2017). Bruxism and dental implant treatment complications: A retrospective

comparative study of 98 bruxer patients and a matched group. *Clinical Oral Implants Research*, 28(7), e1-e9.

16. Chitumalla, R.; Halini Kumari, K.V.; Mohapatra, A.; Parihar, A.S.; Anand, K.S.; and Katragadda, P. (2018). Assessment of survival rate of dental implants in patients with bruxism: A 5-year retrospective study. *Contemporary Clinical Dentistry*, 9(6), 278-282.
17. Mangano, F.G.; Shibli, J.A.; Sammons, R.L.; Iaculli, F.; Piattelli, A.; and Mangano, C. (2014). Short (8-mm) locking-taper implants supporting single crowns in posterior region: A prospective clinical study with 1-to 10-years of follow-up. *Clinical Oral Implants Research*, 25(8), 933-940.
18. Heller, H.; Sreter, D.; Arieli, A.; Beitlitum, I.; Pilo, R.; Levartovsky, S. (2022). Survival and success rates of monolithic zirconia restorations supported by teeth and implants in bruxer versus non-bruxer patients: A retrospective study. *Materials*, 15(3), 1-12.
19. Sadowsky, S.J. (2019). Occlusal overload with dental implants: A review. *International Journal of Implant Dentistry*, 5(1), 1-5.
20. Kopp, S.; Warkentin, M.; Öri, F.; Ottl, P.; Kundt, G.; and Frerich, B. (2012). Section plane selection influences the results of histomorphometric studies: The example of dental implants. *Biomedizinische Technik*, 57(5), 365.
21. Presotto, A.G.C.; Bhering, C.L.B.; Caldas, R.A.; Consani, R.L.X.; Barão, V.A.R.; and Mesquita, M.F. (2018). Photoelastic and finite element stress analysis reliability for implant-supported system stress investigation. *Brazilian Journal of Oral Sciences*, 18, 1-13.
22. Brunski, J.B.; Puleo, D.A.; and Nanci, A. (2000). Biomaterials and biomechanics of oral and maxillofacial implants: Current status and future developments. *The International Journal of Oral & Maxillofacial Implants*, 15(1), 15-46.
23. Omar, A.; Ishak, M.I.; Harun, M.N.; Sulaiman, E.; and Kasim, N.H.A. (2012). Effects of different angulation placement of mini-implant in orthodontic. *Applied Mechanics and Materials*, 121-126, 1214-1219.
24. Ishak, M.I.; Shafi, A.A.; Rosli, M.U.; Khor, C.Y.; Zakaria, M.S.; Abd Rahim, W.M.F.W.; and Jamalludin, M.R. (2017). Biomechanical evaluation of different abutment-implant connections – A nonlinear finite element analysis. *AIP Conference Proceedings*, 1885(1), 020064.
25. Ibrahim, M.I.F.; Rosli, M.U.; Ishak, M.I.; Zakaria, M.S.; Jamalludin, M.R.; Khor, C.Y.; Abd Rahim, W.M.F.W.; Nawi, M.A.M.; and Shahrin, S. (2018). Simulation based optimization of injection molding parameter for meso-scale product of dental component fabrication using response surface methodology (RSM). *AIP Conference Proceedings*, 2030(1), 020078.
26. Boukhlif, A.; Merdji, A.; Roy, S.; Alkhaldi, H.; Abu-Alshaikh, I.; Della, N.; Cristache, C.M.; and Hillstrom, R. (2020). Effect of supporting implants inclination on stability of fixed partial denture: A finite element study. *Proceedings of the Institution of Mechanical Engineers, Part H*, 234(10), 1162-1171.
27. Ouldyerou, A.; Aminallah, L.; Merdji, A.; Mehboob, A.; and Mehboob, H. (2022). Finite element analyses of porous dental implant designs based on 3D

printing concept to evaluate biomechanical behaviors of healthy and osteoporotic bones. *Mechanics of Advanced Materials and Structures*, 1-13.

28. Nawi, M.A.M.; Amin, M.R.; Kasim, M.S.; Izamshah, R. ; Ishak, M.I.; Khor, C.Y.; Rosli, M.U.; Jamalludin, M.R.; and Syafiq, A.K.M. (2019). The influence of spiral blade distributor on pressure drop in a swirling fluidized bed. *IOP Conference Series: Materials Science and Engineering*, 551, 012106.
29. Khor, C.Y.; Ishak, M.I.; Rosli, M.U.; Jamalludin, M.R.; Zakaria, M.S.; Yamin, A.F.M.; Abdul Aziz, A.F.M.; and Abdullah, M.Z. (2017). Influence of material properties on the fluid-structure interaction aspects during molded underfill process. *MATEC Web of Conference*, 97, 01059.
30. Borges Radaelli, M.T.; Idogava, H.T.; Spazzin, A.O.; Noritomi, P.Y.; and Boscato, N. (2018). Parafunctional loading and occlusal device on stress distribution around implants: A 3D finite element analysis. *The Journal of Prosthetic Dentistry*, 120(4), 565-572.
31. Torcato, L.B.; Pellizzer, E.P.; Verri, F.R.; Falcón-Antenucci, R.M.; Júnior, J.F.S.; and de Faria Almeida, D.A. (2015). Influence of parafunctional loading and prosthetic connection on stress distribution: A 3D finite element analysis. *The Journal of Prosthetic Dentistry*, 114(5), 644-651.
32. Yalçın, M.; Kaya, B.; Laçin, N.; and Arı, E. (2019). Three-dimensional finite element analysis of the effect of endosteal implants with different macro designs on stress distribution in different bone qualities. *The International Journal of Oral & Maxillofacial Implants*, 34(3), e43–e50.
33. Schwitalla, A.D.; Abou-Emara, M.; Spintig, T.; Lackmann, J.; and Müller, W.D. (2015). Finite element analysis of the biomechanical effects of PEEK dental implants on the peri-implant bone. *Journal of Biomechanics*, 48(1), 1-7.
34. Gupta, Y.; Iyer, R.; Dommeti, V.K.; Nutu, E., Rana, M.; Merdji, A.; Biswas, J.K.; and Roy, S. (2020). Design of dental implant using design of experiment and topology optimization: A finite element analysis study. *Proceedings of the Institution of Mechanical Engineers, Part H: Journal of Engineering in Medicine*, 235(2), 157-166.
35. Dantas, T.A.; Carneiro Neto, J.P.; Alves, J.L.; Vaz, P.C.S.; and Silva, F.S. (2020). In silico evaluation of the stress fields on the cortical bone surrounding dental implants: Comparing root-analogue and screwed implants. *Journal of the Mechanical Behavior of Biomedical Materials*, 104, 103667.
36. Hussein, F.; Salloomi, K.; Abdulrahman, B.; Al-Zahawi, A.; and Sabri, L. (2019). Effect of thread depth and implant shape on stress distribution in anterior and posterior regions of mandible bone: A finite element analysis. *Dental Research Journal*, 16(3), 200-207.
37. Tribst, J.P.M.; Dal Piva, A.M.d.O.; Borges, A.L.S.; and Bottino, M.A. (2020). Influence of socket-shield technique on the biomechanical response of dental implant: Three-dimensional finite element analysis. *Computer Methods in Biomechanics and Biomedical Engineering*, 23(6), 224-231.
38. Hudieb, M.I.; Wakabayashi, N.; Abu-Hammad, O.A.; and Kasugai, S. (2019). Biomechanical effect of an exposed dental implant's first thread: A three-dimensional finite element analysis study. *Medical Science Monitor*, 25, 3933-3940.

39. Robau-Porrua, A.; Pérez-Rodríguez, Y.; Soris-Rodríguez, L.M.; Pérez-Acosta, O.; and González, J.E. (2020). The effect of diameter, length and elastic modulus of a dental implant on stress and strain levels in peri-implant bone: A 3D finite element analysis. *Bio-Medical Materials and Engineering*, 30, 541-558.
40. Tretto, P.H.W.; dos Santos, M.B.F.; Spazzin, A.O.; Pereira, G.K.R.; and Bacchi, A. (2020). Assessment of stress/strain in dental implants and abutments of alternative materials compared to conventional titanium alloy - 3D non-linear finite element analysis. *Computer Methods in Biomechanics and Biomedical Engineering*, 23(8), 372-383.
41. Tekin, S.; Değer, Y.; and Demirci, F. (2019). Evaluation of the use of PEEK material in implant-supported fixed restorations by finite element analysis. *Nigerian Journal of Clinical Practice*, 22(9), 1252-1258.
42. Elias, D.M.; Valerio, C.S.; de Oliveira, D.D.; Manzi, F.R.; Zenóbio, E.C.; and Seraidarian, P.I. (2020). Evaluation of different heights of prosthetic crowns supported by an ultra-short implant using three-dimensional finite element analysis. *The International Journal of Prosthodontics*, 33(1), 81-90.
43. Azcarate-Velázquez, F.; Castillo-Oyagüe , R.; Oliveros-López, L.-G.; Torres-Lagares, D.; Martínez-González, Á.-J.; Pérez-Velasco, A.; Lynch, C.D.; Gutiérrez-Pérez, J.-L.; and Serrera-Figallo, M.-Á. (2019). Influence of bone quality on the mechanical interaction between implant and bone: A finite element analysis. *Journal of Dentistry*, 88, 103161.
44. Pirmoradian, M.; Naeeni, H.A.; Firouzbakht, M.; Toghraie, D.; Khabaz, M.K.; and Darabi, R. (2020). Finite element analysis and experimental evaluation on stress distribution and sensitivity of dental implants to assess optimum length and thread pitch. *Computer Methods and Programs in Biomedicine*, 187, 105258.
45. Velmurugan, D.; and Alphin, M.S. (2018). Influence of geometric design variable and bone quality on stress distribution for zirconia dental implants - A 3D finite element analysis. *Computer Modeling in Engineering & Sciences*, 117(2), 125-141.
46. Peter, K. (2009). *Theory reference for the mechanical APDL and mechanical applications*. ANSYS, Inc.
47. Chandrupatla, T.; and Belegundu, A. (2021). *Introduction to finite elements in engineering*. Pearson.
48. Budynas, R.G.; and Nisbett, J.K. (2014). *Shigley's mechanical engineering design in SI units*. McGraw-Hill Education.
49. Ayllón, J.M.; Navarro, C.; Vázquez, J.; and Domínguez, J. (2014). Fatigue life estimation in dental implants. *Engineering Fracture Mechanics*, 123, 34-43.
50. Kim, W.H.; Lee, J.-C.; Lim, D.; Heo, Y.-K.; Song, E.-S.; Lim, Y.-J.; and Kim, B. (2019). Optimized dental implant fixture design for the desirable stress distribution in the surrounding bone region: A biomechanical analysis. *Materials*, 12(17), 1-17.
51. Marcián, P.; Wolff, J.; Horáčková, L.; Kaiser, J.; Zikmund, T.; and Borák, L. (2018). Micro finite element analysis of dental implants under different loading conditions. *Computers in Biology and Medicine*, 96, 157-165.
52. Macedo, J.P.; Pereira, J.; Faria, J.; Souza, J.C.M.; Alves, J.L.; López-López, J.; Henriques, B. (2018). Finite element analysis of peri-implant bone volume

affected by stresses around Morse taper implants: Effects of implant positioning to the bone crest. *Computer Methods in Biomechanics and Biomedical Engineering*, 21(12), 655-662.

53. Ishak, M.I.; Daud, R.; Ibrahim, I.; Mat, F.; and Mansor, N.N. (2021). A review of factors influencing peri-implant bone loss. *AIP Conference Proceedings*, 2347(1), 020293.
54. Lee, H.; Park, S.; and Noh, G. (2019). Biomechanical analysis of 4 types of short dental implants in a resorbed mandible. *The Journal of Prosthetic Dentistry*, 121(4), 659-670.
55. Matsuzaki, T.; Ayukawa, Y.; Matsushita, Y.; Sakai, N.; Matsuzaki, M.; Masuzaki, T.; Haraguchi, T.; Ogino, Y.; and Koyano, K. (2019). Effect of post-osseointegration loading magnitude on the dynamics of peri-implant bone: A finite element analysis and in vivo study. *Journal of Prosthodontic Research*, 63(4), 453-459.
56. Dorogoy, A.; Rittel, D.; Shemtov-Yona, K.; and Korabi, R. (2017). Modeling dental implant insertion. *Journal of the Mechanical Behavior of Biomedical Materials*, 68, 42-50.
57. Beschnidt, S.M.; Cacaci, C.; Dedeoglu, K.; Hildebrand, D.; Hulla, H.; Iglhaut, G.; Krennmair, G.; Schlee, M.; Sipos, P.; Stricker, A.; and Ackermann, K.-L. (2018). Implant success and survival rates in daily dental practice: 5-year results of a non-interventional study using CAMLOG SCREW-LINE implants with or without platform-switching abutments. *International Journal of Implant Dentistry*, 4(1), 1-13.
58. Eckert, S.E.; Meraw, S.J.; Cal, E.; and Ow, R.K. (2000). Analysis of incidence and associated factors with fractured implants: A retrospective study. *The International Journal of Oral & Maxillofacial Implants*, 15(5), 662-667.